Cynopterus sphinx activate hypothalamic-pituitary-adrenal (HPA) axis in conspecifics. *J. Comp. Physiol. A*, 2013, **199**, 775–783.

5. Rani, J., *Distress Calls of Sympatric Fruit Bats, Cynopterus sphinx* (*Vahl, 1797*) and *C. brachyotis* (*Müller, 1838*), M Sc Dissertation, The American College, Madurai, 2012.

6. Mariappan, S., Bogdanowicz, W., Raghuram, H., Marimuthu, G., and Emmanuvel Rajan, K., Structure of distress call: implication for specificity and activation of dopaminergic system. *J. Comp. Physiol. A*, 2016, **202**, 55–65.

7. Nathan, P. T., Doss, D. P. S., Isaac, S. S., Balasingh, J., Rajan, K. E., Gopukumar, N. and Subbaraj, R., Mist-net capture and field observation on the short-nosed fruit bat (Chiroptera-Pteropodidae) *Cynopterus sphinx* (Vahl). *J. Bombay Nat. Hist. Soc.*, 2001, **98**, 373–378.

8. Marques, J. T., Ramos Pereira, M. J., Marques, T. A., Santos, C. D., Santana, J., Beja, P. and Palmeirim, J. M., Optimizing sampling design to deal with mist-net avoidance in Amazonian birds and bats. *PLoS ONE*, 2013, **8**, e74505.

9. Wiley, R. H. and Richards, D. G., Adaptations for acoustic communication in birds: sound transmission and signal detection. In *Acoustic Communication in Birds* (eds Kroodsma, D. E. and Miller, E. H.), Academic Press, Ithaca, New York, 1982, vol. 1, pp. 131–181.

10. Bradbury, J. W. and Vehrencamp, S. L., *Principles of Animal Communication*, Sinauer Associates, Sunderland, 2011, p. 697.

11. Eckenweber, M. and Knornschild, M., Responsiveness to conspecific distress calls is influenced by day-roost proximity in bats (*Saccopteryx bilineata*). *R. Soc. Open Sci.*, 2016, **3**, 160151.

12. Carter, G., Schoeppler, D., Manthey, M., Knörnschild, M. and Denzinger, A., Distress calls of a fast-flying bat (*Molossus molossus*) provoke inspection flights but not cooperative mobbing. *PLoS ONE*, 2015, **10**, e0136146.

13. Lučan, R. K. and Šalek, M., Observation of successful mobbing of an insectivorous bat, *Taphozous nudiventris* (Emballonuridae), on an avian predator, *Tyto alba* (Tytonidae). *Mammalia*, 2013, **77**, 235–236.

14. Fenton, M. B., Belwood, J. J., Fullard, J. H. and Kunz, T. H., Responses of *Myotis lucifugus* (Chiroptera: Vespertilionidae) to calls of conspecifics and to other sounds. *Can. J. Zool.*, 1976, **54**, 1443–1448.

15. Avery, M. I., Racey, P. A. and Fenton, M. B., Short distance location of hibernaculum by little brown bats. *J. Zool.* (*London*), 1984, **204**, 588–590.

16. Russ, J. M., Jones, G. and Racey, P. A., Intraspecific responses to distress calls of the pipistrelle bat, *Pipistrellus pipistrellus. Anim. Behav.*, 1998, **55**, 705–713.

17. Russ, J. M., Jones, G., Mackie, I. J. and Racey, P. A., Interspecific responses to distress calls in bats (Chiroptera: Vespertilionidae): a function for convergence in call design? *Anim. Behav.*, 2004, **67**, 1005–1014.

18. Ryan, M. J., Clark, D. B. and Lackey, J. A., Response of *Artibeus lituratus* (Chiroptera: Phyllostomidae) to distress calls of conspecifics. *J. Mammal.*, 1985, **66**, 179–181.

19. Gopukumar, N., Elangovan, V., Sripathi, K., Marimuthu, G. and Subbaraj, R., Foraging behavior of the Indian short-nosed fruit bat *Cynopterus sphinx. Z. Saugetierk.*, 1999, **64**, 187–191.

20. Raghuram, H., Gopukumar, N. and Sripathi, K., Presence of single as well double clicks in the echolocation signals of a fruit bat *Rousettus leschenaulti* (Chiroptera: Pteropodidae). *Folia Zool.*, 2007, **56**, 33–38.

21. Rajan, K. E., Nair, N. G. and Subbaraj, R., Seasonal food preference on the Indian short-nosed fruit bat *Cynopterus sphinx* (Vahl) (Chiroptera: Pteropodidae). *J. Bombay Nat. Hist. Soc.*, 1999, **96**, 24–27.

22. Chen, Z., Meng, Y., Zhou, F. and Li, Y., Activity rhythms and food habits of Leschenault's rousette (*Rousettus leschenaulti*) in Hainan Island. *Acta Theriol. Sinica,* 2007, **27**, 112–119.

23. August, P. X. V., Distress calls in *Artibeus jamaicensis*: ecology and evolutionary implications. In *Vertebrate Ecology in the Northern Neotropics* (ed. Eisenberg, J. F.), Smithsonian Institute, Washington, 1979, pp. 151–160.

Response of methane diffusion in varying degrees of deformed coals to different solvent treatments

Pengpeng Li[1,2,3,4], Xiaodong Zhang[1,*] and Shuo Zhang[1]

[1]School of Energy Science and Engineering, Henan Polytechnic University, Jiaozuo, Henan Province 454000, China
[2]Northwest Institute of Eco-Environment and Resources, Chinese Academy of Sciences, Lanzhou 730000, China
[3]Key Laboratory of Petroleum Resources of Gansu Province/ Key Laboratory of Petroleum Resources, Chinese Academy of Sciences, Lanzhou 730000, China
[4]University of Chinese Academy of Sciences, Beijing 100049, China

In the communication, we analysed four semi-anthracite coals with different degrees of deformation from the Huoerxinhe colliery in China that were extracted by tetrahydrofuran (THF) and carbon disulphide (CS_2), and treated with hydrochloric acid (HCl) solution. Low-temperature nitrogen adsorption, water contact angle measurement and methane diffusion of untreated coals and their residues were carried out. As well, mineral composition of untreated coals and their residues treated with HCl are performed. Overall, compared with untreated coals, specific surface area has increased tendency after THF and CS_2 extraction due to the removal of the soluble organic components in coal, depends jointly on mineral types and their respective content after HCl treatment. Regardless of coal un- or treated by solvents, diffusion coefficient grows with increasing coal deformation. Further study shows that the diffusion coefficient of

*For correspondence. (e-mail: z_wenfeng@163.com)

coal with same deformation increases as follows: HCl treated coal residues, THF extracted coal residues, untreated coals, CS$_2$ extracted coal residues. The aforementioned phenomena result from two aspects: on one hand, the enlargement of pore after solvent treatment reduces the collision between methane molecule and pore walls, thus improving the efficient of methane diffusion; on the other hand, pore is narrowed or even blocked completely due to the retention of foreign matters, which increases the resistance of methane diffusion. Therefore, methane diffusion after solvent treatment is jointly dependent on pore change because of the removal of soluble components and the retention of foreign matters.

Keywords: Deformed coal, diffusion coefficient, pore structure, solvent treatment, wettability.

MOST coal-bearing basins in China experienced superposition of one- or multi-phase and different-scale geological tectonic movements. As a result, the original coal beddings near the geological structures in those coal basins were destroyed due to the shearing or squeezing actions, and subsequently formed various types of deformed coals[1]. Extensive studies demonstrate that almost all coal-gas outburst accidents happen in deformed coal seams. Neither the coal bed methane (CBM) recovery nor the gas extraction from underground coal seams ever achieved a good result[2]. A coal reservoir is a typical dual-porosity media composed of pore and fracture system[3]. Generally, CBM migration is regarded a multi-scale mass transport process, including desorption in the matrix diffusion in the pore system and finally seepage within the fracture system[4]. The methane production rate during the later part of the CBM reservoir's life, is considerably controlled by diffusion[5,6]. Therefore, improving methane diffusion performance is of great significance for enhancing CBM recovery and preventing coal-gas outburst. Hydraulic fracturing, the most widely used reservoir simulation technique, has been applied to bettering coal seam penetration via generating a number of new fractures and enlarging the width of inherent fractures. However, trapped fracturing fluid and the expansion of clay minerals are bound to cause plugging of pore and the change of wettability[4], which affects/reduces methane diffusion performance.

Solvent extraction is routinely used to study coal structure. Identification and analysis of extracted products provide a wealth of information about coal structure that improves the understanding of integrated chemical/structural coal models[7]. Coal is considered a three-dimensional macromolecule composed of condensed aromatic nuclei containing functional groups and side chains that can be soluble in organic solvents[8]. Removal of soluble organic fractions in coal produce porous and cause physical, chemical and adsorption changes[9–13]. Considering the fact that changes in pore structure are closely related to methane diffusion, diffusion performance after organic solvent extraction is imperative to research.

The current technologies used for methane diffusion assessment are performed under high pressure, which easily destroys the pore structure in long tests and cannot fully reflects authentic pore structure characteristics. When pressure is more than 2 MPa, in addition to the methane in free and sorption states, there is methane in the solid solution state that is notably difficult to desorb[14]. Marked hysteresis loops of methane adsorption–desorption isotherm in high-pressure stage confirms this phenomenon objectively[15]. In this work, four coal samples with different degrees of deformation were extracted with tetrahydrofuran (THF) and carbon disulphide (CS$_2$) and treated by hydrochloric acid (HCl) (20 wt%). In order to study the change in pore structure after solvent treatments, methane diffusion experiments were performed at atmospheric pressure. And the pore structure parameters of coal samples before and after different solvent treatments were measured using low-temperature liquid nitrogen adsorption which is an effective method to characterize the pore structure of porous medium[16]. Then, the influencing factors of diffusion were discussed. These experimental results may allow us to understand the mechanism of solvent extraction on methane diffusion.

The semi-anthracite coal samples used for this study were obtained from the early Permian No. 3 coal seam in Huoerxinhe Colliery, Shanxi Province, China. Fresh blocks of coal with different degrees of deformation (Figure 1), i.e. undeformed (I), cataclastic coal (II), granulated coal (III), mylonitized coal (IV), newly exposed by active mining operations, were firstly selected, immediately placed in sample bags in underground colliery, and transported to the laboratory at room temperature (approximately 20°C). The features of coal samples with different degrees of deformation are described by Li *et al.*[17].

Coal samples were smashed and sieved to size fraction of 80–100 mesh. After drying at 105°C in a drying oven to a constant weight (the difference of weight of the last two times less than 0.001 g). The coal samples (20 g) were treated with THF and CS$_2$ for 12 h and were soaked with HCl for 72 h at room temperature (approximately 20°C) in conical flasks sealed by plastic sheeting. The treated liquids were transferred into test tubes, and coal residues were dried to a constant weight at 105°C for further experiments. The solid residues after organic solvents extraction are the extracted coal residues, and after HCl treatment they are called treated coal residues. Proximate analyses of all samples were conducted according to the China National Standard GB/T 212-2008. The results of proximate analyses were presented in Table 1.

The experimental apparatus is shown schematically in Figure 2. Brief descriptions of the experimental
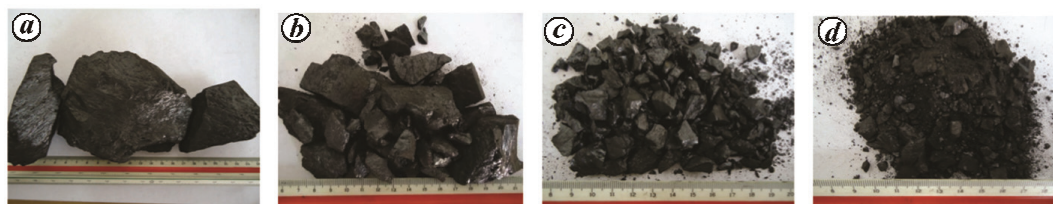
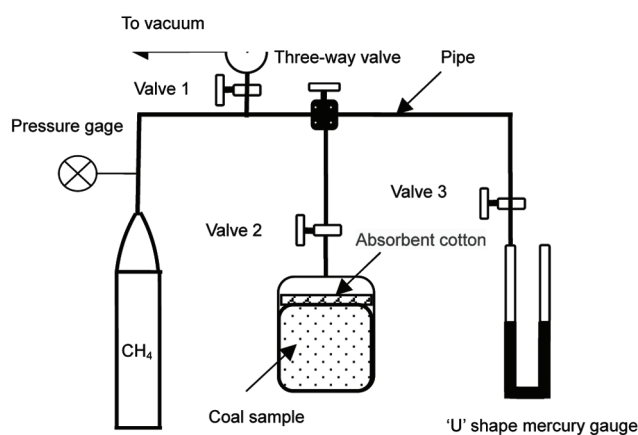**Figure 1.** *a*, Undeformed coal; *b*, Cataclastic coal; *c*, Granulated coal; *d*, Mylonitized coal.

Figure 2. Schematic plot of experimental apparatus.

Table 1. Results from proximate analysis of all coal samples

Sample ID	Proximate analysis (wt%)			
	Moisture	Ash	Volatile	Fixed carbon
I	1.09	9.91	11.15	77.87
II	0.88	11.11	11.39	76.73
III	0.74	8.41	11.43	79.42
IV	1.02	10.25	11.23	77.51
I-THF	1.06	11.41	12.03	75.51
II-THF	1.19	11.86	12.26	74.70
III-THF	1.11	11.71	12.11	75.09
IV-THF	1.17	9.66	12.04	77.14
I-CS$_2$	0.70	10.34	11.14	77.82
II-CS$_2$	0.69	13.15	11.13	75.04
III-CS$_2$	0.90	8.55	11.27	79.29
IV-CS$_2$	0.79	10.85	11.20	77.16
I-HCl	4.73	7.38	12.13	75.77
II-HCl	7.60	8.09	13.07	71.24
III-HCl	3.93	7.38	12.13	76.57
IV-HCl	4.56	9.00	12.02	74.93

Where I-THF refers to the undeformed coal extracted by THF, others in Table 1 are by analogy likewise.

procedures are as follows. First, coal samples were weighted 3.5 g using a high-precision electronic balance with a precision of 0.1 mg and were loaded into sample cells. A layer of absorbent cotton was used to cover crushed coal samples to prevent them from moving into pipes. Before methane diffusion measurements, it was ensured that the system was air-tight. After this step, the

system was vacuumed with valves 1 and 2 open. When the operation of the vacuum finished, methane was expanded into sample cell for 2 h with valve 2 open, which aims to reach adsorption equilibrium. Then, valve 2 was turned off and values 1 and 3 were turned on in turn, and the system was again vacuumed. Following this, with valves 1 and 3 open, methane diffusion experiment was performed and the amount of methane diffusion during different time intervals was recorded. The same procedure measuring the amount of methane diffusion was repeated again. If the difference of two test values was less than 1 mmHg, the average test value was adopted. Once the difference was higher than 1 mmHg, the experiment must be carried out again as described in the preceding steps.

The pore structure parameters of all coal samples were determined using a Micromeritic TriStar II 3020 automatic surface area and porosity analyzer. The coal samples (1 g) were analysed using liquid nitrogen. The temperature of each sample was set at 77 K (liquid N$_2$) in order to quantify N$_2$ gas adsorption in coal. It should be noted that opened pores were only studied because liquid nitrogen cannot enter into the closed pores that had little impact on methane diffusion[16]. The instrument's software automatically generated adsorption isotherms and calculated specific surface areas (BET layer adsorption formula) and pore volumes (BJH model).

The water contact angle was measured by Contact Angle Tester (JC2000C1). Coal residues (4 g) were pressed into the cylindrical slice with a diameter of 5 cm by an automatically high-pressure briquette machine before measurement. A water droplet of 2 ul was set onto the cylindrical slice and the shape of the water droplet was recorded by a charge-coupled device camera. The water contact angle was then calculated by a software using angle measurement.

The type of minerals and their respective percentage content of the untreated coals and HCl treated coal residues were determined using the EMITECH K1050X plasma asher and Rigaku D/max-2500/PC X-ray diffractometer. Quantitative determination of minerals in low-temperature ashing samples was performed following the methods described by Dai *et al.*[18].

The extraction yield of organic solvent was calculated using eq. (1), and the results are listed in Table 2. Extraction yield augments with increasing coal deformation

after extraction. A greater pore provide more opportunity for the solvent has to contact coal materials, thereby increasing the production of soluble organic matters. Further, tectonic stress, usually in the form of mechanical force or kinetic energy, acts on coal's macromolecular structure by developing two different orientations. On one hand, the aromatization degree increases and the coal molecular structure units become closely packed. On the other hand, the side chains and functional groups with lower bond energy in the coal aromatic structure fall out and free radicals with small molecular weight are formed[19] (see Table 2).

The extraction yield is higher after extraction with THF than CS_2. Due to its stronger polarity, THF can extract higher content of nonhydrocarbon constituents such as nitrogen, sulphur and oxygen compounds besides alkanes and arenes[20]

$$E = \frac{(W - W_1) \times 100}{(100 - A_{ad} - M_{ad}) \times W / 100}, \qquad (1)$$

where E is the extraction yield, W and W_1 are the qualities of the untreated coals and extracted coal residues, A_{ad} and M_{ad} are the ash and moisture contents of the untreated coals.

Table 2. Extraction yield of coals with various degrees of deformation after THF and CS_2 extractions

Sample ID	Extraction yield	Sample ID	Extraction yield
I-THF	0.69	I-CS_2	0.42
II-THF	0.81	II-CS_2	0.51
III-THF	0.93	III-CS_2	0.53
IV-THF	1.00	IV-CS_2	0.57

Table 3. Pore structure parameters of coal samples before and after different solvent treatments

Sample ID	Total SSA (m^2/g)	SSAs of different segments (m^2/g)		
		Micropore	Mesopore	Macropore
I	0.43	0.20	0.17	0.06
II	0.28	0.11	0.12	0.05
III	0.61	0.32	0.18	0.11
IV	0.54	0.26	0.18	0.10
I-THF	0.34	0.14	0.17	0.03
II-THF	0.72	0.52	0.16	0.04
III-THF	0.26	0.16	0.06	0.04
IV-THF	0.73	0.42	0.20	0.11
I-CS_2	0.77	0.45	0.18	0.14
II-CS_2	0.48	0.24	0.14	0.10
III-CS_2	0.57	0.22	0.19	0.16
IV-CS_2	0.84	0.43	0.21	0.20
I-HCl	0.88	0.56	0.19	0.12
II-HCl	0.68	0.45	0.14	0.09
III-HCl	1.39	0.86	0.22	0.31
IV-HCl	0.31	0.13	0.15	0.03

In this work, the classification of pore sizes follows the literature[21], defining micropore width as <2 nm, the range of mesopore width as 2–50 nm, macropore width as >50 nm. Figure 3 shows a positive linear correlation between pore volume and specific surface area (SSA). For simplicity, the following description takes SSA for instance. Pore structure parameters obtained by low-temperature liquid nitrogen adsorption are summarized in Table 3.

Coal contains a certain number of minerals, mainly clay minerals (kaolin, illite and nacrite) and carbonate minerals (siderite, calcite and dolomite), corresponding to the results (Table 4) that the percentage of clay minerals and carbonate minerals accounts for more than 80% (wt%) of all minerals in untreated coals, even exceed 90% for granulated and mylonitized coals. Carbonate minerals filling pores almost are completely dissolved after HCl treatment resulting in forming new pores and enlarging existed pores. Most of the clay minerals are water-expandable, their swelling is bound to block pores. Therefore, it is thought that changes in SSA after HCl treatment depend mainly on changes in pore due to dissolution of carbonate minerals and the swelling of clay minerals in coal. Ash content in coal is mainly the residue of minerals burned at 850°C high temperature, it can be used to characterize minerals content. Therefore, it is deduced that the ash content of coals treated by HCl is the residue of clay minerals, which is consistent with the fact that the ash content of coals decreases obviously after HCl treatment. From the results given Tables 1 and 4, after HCl treatment, for undeformed and cataclastic coals, total SSA and SSAs of different segments have trend to ascend mainly due to the dissolution of carbonate minerals; for mylonitized coal, total SSA and SSAs of different segments have trend to descent as a result of the swelling of clay minerals; for granulated coal, although
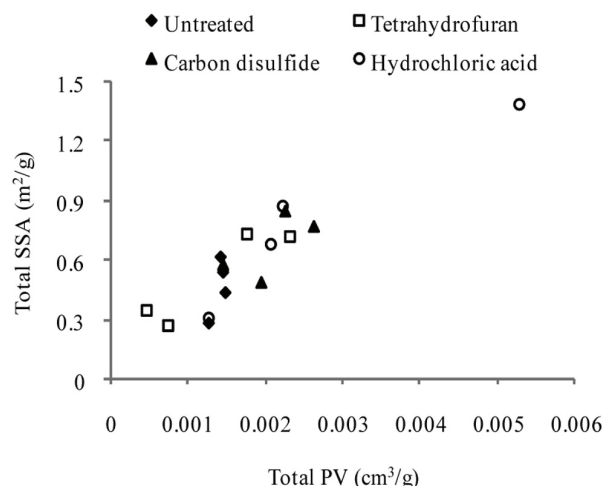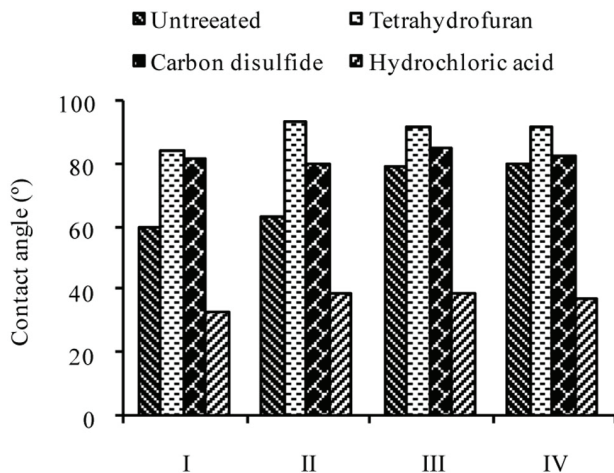

Figure 3. Relationship between pore volume and specific surface area.

Table 4. Mineral types and their respective content of coal samples before and after HCl treatment

Type	Sample ID							
	I	I-HCl	II	II-HCl	III	III-HCl	IV	IV-HCl
Clay minerals	35.9	64.8	58.1	81.3	94.0	99.6	93.2	99.6
Carbonate minerals	41.1	2.7	10.7	0	6.0	0	3.4	0
Other minerals	23.0	32.5	31.2	18.7	0	0.4	3.4	0.4

Figure 4. Water contact angles of coal samples before and after different solvents treatments.

the proportion of clay minerals is highest, these parameters all rise possibly because of low content of clay minerals or the uneven distribution of clay minerals in coal samples.

The removal of extractable organic fractions from coal via organic solvent extraction causes the enlargement and opening of previously existed or closed pores, resulting in increased SSA[9]. Overall, regardless of coal deformation, after extraction with THF and CS$_2$, total micropore and mesopore SSAs become larger, the macropore SSA decreases after extraction with THF but it increases after CS$_2$ extraction. These changes may be caused by the differences in extraction efficiency and the kinetics of penetration between THF and CS$_2$.

Figure 4 shows that compared to untreated coals, the water contact angles of HCl treated coal residues are noticeably lower, which is consistent with the fact that moisture increases from proximate analysis results. This happens because: (1) the clay minerals swell in HCl solution, (2) the ester in coals exposed in the solution is protonated, and certain carboxyl groups with strong hydrophilicity are produced simultaneously. The water contact angles of THF and CS$_2$ extracted residues are larger than untreated coals, suggesting that coals become more hydrophobic after organic solvents extraction. A larger contact angle is observed after extraction with THF compared with CS$_2$, suggesting that the extractable

organic fractions include more hydrophilic active groups using THF.

Methane migration in coal particle is assumed to be concentration gradient-driven and is usually modelled by Fick's second law for spherically symmetric flow[22]

$$\frac{\partial c}{\partial t} = D\left(\frac{\partial^2 c}{\partial r^2} + \frac{2}{r}\frac{\partial c}{\partial r}\right), \tag{2}$$

where c is the methane concentration, t the time, D the diffusion coefficient, which is thought to be independent of concentration and location in coal particle and r is the sphere radius. The model assumes spherical and homogeneous coal particle with identical radius and smooth surface. And the analytical solution is obtained by Crank as shown in eq. (3). It is reported that the single parameter model has been successfully used to describe gas diffusion for high rank coals[23]

$$\frac{Q_t}{Q_\infty} = 1 - \frac{6}{\pi^2}\sum_{n=1}^{\infty}\frac{1}{n^2}\exp\left(\frac{-Dn^2\pi^2 t}{r^2}\right), \tag{3}$$

where Q_t is the total amount of methane desorbed amount within time t and Q_∞ is the total amount of methane desorbed at indefinite time. For short times ($t < 600$ s), eq. (3) can be simplified (eq. (4)) to estimate the diffusion coefficient[5]

$$\frac{Q_t}{Q_\infty} = \frac{6}{r}\sqrt{\frac{Dt}{\pi}} = k\sqrt{t} \tag{4}$$

It is obtained that $D = \pi k^2 r^2/36$.

Diffusion coefficients of coals before and after solvents treatment are summarized in Figure 5. After solvents treatment, the diffusion coefficient of coal with same degree of deformation increases as follows: HCl treated coal residues < THF extracted coal residues < untreated coals < CS$_2$ extracted coal residues. As a whole, diffusion coefficient shows a growing tendency with increased deformation for untreated coals. Similar trend is also observed for deformed coals.

The essence of methane diffusion is its irregular thermal motion based on the kinetic theory. Generally, methane diffusion in pore is considered as a combination

of three types of diffusion: Knudsen diffusion, surface diffusion and bulk diffusion[5,24,25]. Knudsen diffusion, whose resistance of flow includes the intermolecular collisions and methane colliding with pore walls, occurs when the pore diameter is greater than the molecular diameter. Bulk diffusion takes place when pore diameter is greater than the mean free path of methane molecule, its resistance comes mainly from collision between methane molecule. Surface diffusion is much smaller than the Knudsen diffusion and usually ignored at room temperature. According to eq. (5), the mean free path of methane molecule is 53.1 nm at 0.1 MPa and 293 K. Thus, it is thought that Knudsen diffusion mainly takes place in micropore and mesopore, and bulk diffusion primarily occurs in macropore. Overall, methane diffusion in pores is the combined outcome of above two types of diffusion.

$$\lambda = \frac{KT}{\sqrt{2}\pi d^2 P},$$ (5)

where K is the Boltzmann constant, 1.38×10^{-23} J/K, T the experimental temperature, d the effective diameter of methane molecular and P is the experimental pressure.

It is reported that pore changes are linked with coal swelling, as well as the mobility of macromolecules within open pores in coal after organic solvents extractions[26,27]. For untreated coals, the pore develops increasingly as coal deformation increases, which is more conductive to provide more solvent seepage channels for extracting soluble organic matters in coal. Before and after solvents extraction, regardless of coal deformation, diffusion coefficient can be arranged in a descending order: CS_2 extracted coal residues > untreated coals > THF extracted coal residues > HCl treated coal residues.
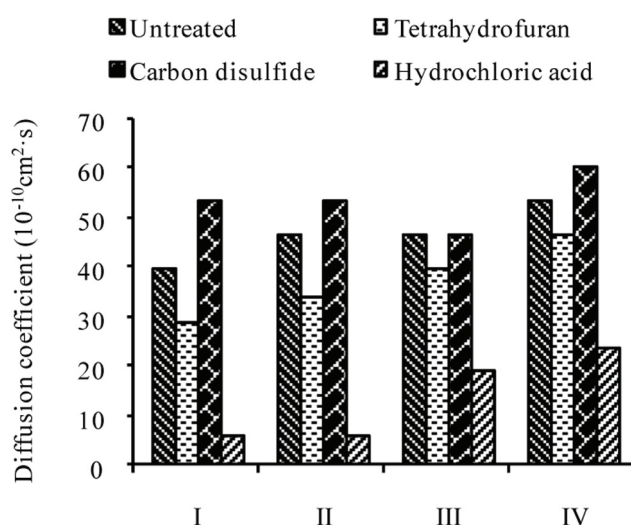

Figure 5. Diffusion coefficients of coals before and after different solvents treatments.

Further, taking mylonitized coal for instance, after extraction with THF, micropore present obviously grows, but macropore reduces significantly. This is due to the retention of highly viscous THF (0.58 mPa•s at 20°C) in macropore walls which forms the more new micropore or mesopore and narrows the mass transport channels. However, after extraction with CS_2, pore of different segments improve because less viscous of CS_2 (0.363 mPa•s at 20°C) is easier to carry soluble organic matters out of the coal and CS_2 retention in pore walls is less. Further, the increased pore, especially macropore reduces the resistance of methane diffusion. These interesting findings indicate that the modification of coal is more conducive to methane diffusion after extraction with CS_2 than THF. After HCl treatment, the swelling of clay minerals narrows and even blocks the pore.

Regardless of the effect of solvent treatment, diffusion coefficient with different degrees of coal deformation can be arranged in a descending order: mylonitized coal > granulated coal > cataclastic coal > undeformed coal, which indicates solvent treatment causes a limited change on methane diffusion compared with original difference among coals with different degrees of deformation.

Wettability can be characterized by the water contact angle[28]. Coal wettability boosts after HCl treatment. Substantial experiments demonstrate that water molecule getting into the coal pore can influence the methane desorption characteristics via the following two aspects: on one hand, the desorption performance weakens significantly due to high capillary pressure constraint; on the other hand, the existence of water on coal pore surface occupies some pore, which narrows the mass transport channels and increase the resistance of methane migration[24]. Clarkson and Bustin also draw a conclusion that the desorption rate of dry coal become larger compared with wet coal[29]. In addition, although the carbonate minerals from coal can be dissolved using acid fluid for CBM development, the dramatic variation of wettability makes it difficult for this fluid to be recovered during clean-up phase, the residual fluid in coal, causes the swelling of clay minerals giving rise to irreversible reservoir damage and thereby reducing the CBM diffusivity and production. Therefore, the change of coal wettability after HCl treatment plays a key role in methane adsorption and diffusion behaviours, which should be paid greater importance.

(1) Overall, compared with untreated coals, specific surface area has increased tendency after THF and CS_2 extraction due to the removal of the soluble organic components in coal, depends jointly on mineral types and their respective content after HCl treatment.

(2) After different solvent treatments, the effect of removing soluble organic fractions or the dissolution and swelling of minerals on methane diffusion is limited and lower compared with the original difference among

various degrees of coal deformation, so diffusion coefficient shows a growing tendency with increased coal deformation.

(3) Regardless of coal deformation, diffusion coefficient varies significantly after solvent treatment, due to two aspects: on one hand, the enlargement of pore after solvent treatment reduces the collision between methane molecule and pore walls, thus improving the efficient of methane diffusion; on the other hand, pore is narrowed or even blocked completely due to the retention of foreign matters from treated fluids or due to reaction between solvent and substances in coal, which increases the resistance of methane diffusion. Therefore, methane diffusion depends on pore space after solvent treatment.

1. Zhang, X. D., Li, P. P., Yang, Y. H. and Du, Z. G., Characteristics of P-wave and S-wave times and their relationship with Young's modulus of coals with different degrees of deformation. *Arab. J. Geosci.*, 2017, **10**, 75; doi:10.1007/s12517-017-2855-x.
2. Meng, Z. P., Liu, S. S. and Li, G. Q., Adsorption capacity, adsorption potential and surface free energy of different structure high rank coals. *J. Petrol. Sci. Eng.*, 2016, **146**, 856–865.
3. Warrant, J. E. and Root, P. J., The behavior of naturally fractured reservoirs. *Soc. Pet. Eng. J.*, 1963, **3**, 245–255.
4. Kang, Y. L., Huang, F. S., You, L. J., Li, X. C. and Gao, B., Impact of fracturing fluid on multi-scale mass transport in coalbed methane reservoirs. *Int. J. Coal Geol.*, 2016, **154–155**, 123–135.
5. Pillalamarry, M., Harpalani, S. and Liu, S. M., Gas diffusion behavior of coal and its impact on production from coalbed methane reservoirs. *Int. J. Coal Geol.*, 2011, **86**, 342–348.
6. Etminan, S. R., Javadpour, F., Mainia, B. B. and Chen, Z. X., Measurement of gas storage processes in shale and of the molecular diffusion coefficient in kerogen. *Int. J. Coal Geol.*, 2014, **123**, 10–19.
7. Shui, H. F., Wang, Z. C. and Gao, J. S., Examination of the role of CS_2 in the CS_2/NMP mixed solvent to coal extraction. *Fuel Process. Technol.*, 2006, **87**, 185–190.
8. Pan, J. N., Zhu, H. T., Hou, Q. L., Wang, H. C. and Wang, S., Macromolecular and pore structure of Chinese tectonically deformed coal studied by atomic force microscopy. *Fuel*, 2015, **139**, 94–101.
9. Agnieszka, F., Maria, M., Simon, C., Brassell, A. S. and Flynn, P., Extractability of biomarkers from high- and low-vitrinite coals and its effect on the porosity of coal. *Int. J. Coal Geol.*, 2013, **107**, 141–151.
10. Zhang, X. D., Miao, S. L., Wang, G. X., Qin, Y. and Sang, S. X., Investigation on pore structures of a medium volatile bituminous coal with solvent extraction tests. *Energ. Explor. Exploit.*, 2013, **31**, 337–352.
11. Ji, H. J., Li, Z. H., Peng, Y. J., Yang, Y. L., Tang, Y. B. and Liu, Z., Pore structures and methane sorption characteristics of coal after extraction with tetrahydrofuran. *J. Nat. Gas Sci. Eng.*, 2014, **19**, 287–294.
12. Vasilakos, N. P., Dobbs, J. M. and Parisl, A. S., Solvent effects in supercritical extraction of coal. *Ind. Eng. Chem. Process Design Dev.*, 1985, **24**, 121–128.
13. Shui, H., Norinaga, K. and Iino, M., Effect of tetrabutylammonium acetate addition on the aggregation of coal molecules at solution and solid states. *Energ. Fuel.*, 2001, **15**, 487–491.
14. Alexeev, A., Ulyanova, E., Starikov, G. and Kovriga, N., Latent methane in fossil coals. *Fuel*, 2004, **83**, 1407–1411.
15. Jessen, K., Tang, G. Q. and Kovscek, A. R., Laboratory and simulation investigation of enhanced coalbed methane recovery by gas injection. *Transp. Porous Media*, 2008, **73**, 141–159.
16. Nie, B. S., Liu, X. F., Yang, L. L., Meng, J. Q. and Li, X. C., Pore structure characterization of different rank coals using gas adsorption and scanning electron microscopy. *Fuel*, 2015, **158**, 908–917.
17. Li, P. P., Zhang, X. D. and Zhang, S., Structures and fractal characteristics of pores in low volatile bituminous deformed coals by low-temperature N_2 adsorption after different solvents treatments. *Fuel*, 2018, **224**, 661–675.
18. Dai, S. F. *et al.*, Chemical and mineralogical compositions of silicic, mafic, and alkali tonsteins in the late Permian coals from the Songzao Coalfield, Chongqing, Southwest China. *Chem. Geol.* 2011, **282**, 29–44.
19. Ju, Y. W., Jiang, B., Hou, Q. L., Tan, Y. L., Wang, G. L. and Xiao, W. J., Behavior and mechanism of the adsorption/desorption of tectonically deformed coals. *Chin. Sci. Bull.*, 2009, **54**, 88–94.
20. Zhang, X. D., Zhang, S., Kong, L. F. and Wei, C. Y., Study on group composition and chemical composition of extracted gas coal of Jinyuan coalmine in Shandong Province. *Coal Convers.*, 2015, **38**, 1–4, 68.
21. Everett, D. H., Manual of symbols and terminology for physicochemical quantities and units, Appendix II: Definitions, terminology and symbols in colloid and surface chemistry. Part I. *Pure Appl. Chem.*, 1972, **31**, 577–638.
22. Ni, C. and San, J., Mass diffusion in a spherical microporous particle with thermal effect and gas-side mass transfer resistance. *Int. J. Heat Mass Transf.*, 2000, **43**, 2129–2139.
23. Shi, J. Q. and Durucan, S., A bidisperse pore diffusion model for methane displacement desorption in coal by CO_2 injection. *Fuel*, 2003, **82**, 1219–1229.
24. Wang, K., Zang, J., Feng, Y. F. and Wu, Y. Q., Effects of moisture on diffusion kinetics in Chinese coals during methane desorption. *J. Nat. Gas Sci. Eng.*, 2014, **21**, 1005–1014.
25. Pan, Z. J., Connell, L. D., Camilleri, M. and Connelly, L., Effects of matrix moisture on gas diffusion and flow in coal. *Fuel*, 2010, **89**, 3207–3217.
26. Pajak, J. and Marzec, A., Influence of pre-swelling on extraction of coal. *Fuel*, 1983, **62**, 979–980.
27. Marzec, A. and Kisielow, W., Mechanism of swelling and extraction and coal structure. *Fuel*, l983, **62**, 977–979.
28. Wei, Q., Ding, Y. L., Nie, Z. R., Liu, X. G. and Li, Q. Y., Wettability, pore structure and performance of perfluorodecyl-modified silica membranes. *J. Membrane Sci.*, 2014, **455**, 114–122.
29. Clarkson, C. R. and Bustin, R. M., The effect of pore structure and gas pressure upon the transport properties of coal: a laboratory and modeling study. 2. Adsorption rate modeling. *Fuel*, 1999, **78**, 1345–1362.